


## Design of $NO_2$ photoacoustic sensor with high reflective mirror based on low power blue diode laser

Hua-Wei Jin(靳华伟), Pin-Hua Xie(谢品华), Ren-Zhi Hu(胡仁志), Chong-Chong Huang(黄崇崇), Chuan Lin(林川), Feng-Yang Wang(王凤阳)

**Citation:**Chin. Phys. B . 2020, 29(6): 060701 . **doi:** 10.1088/1674-1056/ab8376
Journal homepage: http://cpb.iphy.ac.cn; http://iopscience.iop.org/cpb

**What follows is a list of articles you may be interested in**

---

## Atmospheric $N_2O$ gas detection based on an inter-band cascade laser around 3.939 μm

Chun-Yan Sun(孙春艳), Yuan Cao(曹渊), Jia-Jin Chen(陈家金), Jing-Jing Wang(王静静), Gang Cheng(程刚), Gui-Shi Wang(王贵师), Xiao-Ming Gao(高晓明)

Chin. Phys. B . 2020, 29(1): 010704 . **doi:** 10.1088/1674-1056/ab5ef6

## Calibration and data restoration of light field modulated imaging spectrometer

Li-Juan Su(苏丽娟), Qiang-Qiang Yan(严强强), Yan Yuan(袁艳), Shi-Feng Wang(王世丰), Yu-Jian Liu(刘宇健)

Chin. Phys. B . 2018, 27(8): 080702 . **doi:** 10.1088/1674-1056/27/8/080702

## Modeling and analysis for the image mapping spectrometer

Yan Yuan(袁艳), Xiao-Ming Ding(丁晓铭), Li-Juan Su(苏丽娟), Wan-Yue Wang(王婉悦)

Chin. Phys. B . 2017, 26(4): 040701 . **doi:** 10.1088/1674-1056/26/4/040701

## Daily variation of radon gas and its short-lived progeny concentration near ground level and estimation of aerosol residence time

M Mohery, A M Abdallah, A Ali, S S Baz

Chin. Phys. B . 2016, 25(5): 050701 . **doi:** 10.1088/1674-1056/25/5/050701

## Theoretical analysis of stack gas emission velocity measurement by optical scintillation

Yang Yang, Dong Feng-Zhong, Ni Zhi-Bo, Pang Tao, Zeng Zong-Yong, Wu Bian, Zhang Zhi-Rong

Chin. Phys. B . 2014, 23(4): 040703 . **doi:** 10.1088/1674-1056/23/4/040703

---

# Design of $NO_2$ photoacoustic sensor with high reflective mirror based on low power blue diode laser*

Hua-Wei Jin(靳华伟)[1,2,6], Pin-Hua Xie(谢品华)[1,3,4,5,†], Ren-Zhi Hu(胡仁志)[1,2,‡], Chong-Chong Huang(黄崇崇)[1,2], Chuan Lin(林川)[1], and Feng-Yang Wang(王凤阳)[1,2]

[1] *Key Laboratory of Environmental Optics & Technology, Anhui Institute of Optics and Fine Mechanics, Chinese Academy of Sciences (CAS), Hefei* 230031, *China*

[2] *University of Science and Technology of China, Hefei* 230026, *China*

[3] *CAS Center for Excellence in Regional Atmospheric Environment, Institute of Urban Environment, Chinese Academy of Sciences, Xiamen* 361000, *China*

[4] *Institutes of Physical Science and Information Technology, Anhui University, Hefei* 230601, *China*

[5] *University of Chinese Academy of Sciences, Beijing* 100049, *China*

[6] *Anhui Key Laboratory of Mine Intelligent Equipment and Technology, Anhui University of Science and Technology, Huainan* 232001, *China*

(Received 9 February 2020; revised manuscript received 13 March 2020; accepted manuscript online 26 March 2020)

An $NO_2$ photoacoustic sensor system with a high reflective mirror based on a low power blue diode laser is developed in this work. The excitation power is enhanced by increasing the number of reflections. Comparing with a traditional photoacoustic system, the pool constant is improved from 300.24 (Pa·cm)/W to 1450.64 (Pa·cm)/W, and the signal sensitivity of the photoacoustic sensor is increased from 0.016 μV/ppb to 0.2562 μV/ppb. The characteristics of temperature and humidity of the new photoacoustic sensor are also obtained, and the algorithm is adjusted to provide a quantitative response and drift of the resonance frequency. The results of this research provide a new method and concept for further developing the $NO_2$ photoacoustic sensors.

**Keywords:** $NO_2$, photoacoustic sensor, high reflective mirror, blue diode laser

**PACS:** 07.88.+y, 07.60.Rd, 42.60.Da, 43.58.Kr **DOI:** 10.1088/1674-1056/ab8376

## 1. Introduction

Photoacoustic spectroscopy (PAS) is based on the photoacoustic effect. No radiation relaxation occurs when converting part or all of the absorbed light energy into heat. The resulting pressure wave then radiates outward. Gas detection refers to exploring the source of heat power density with periodic changes formed through the absorption and modulation of light energy by gas molecules in a closed cavity, thus causing the gas pressure to periodically change in the cavity and stimulating the sound signal. The cavity is generally considered to radiate ultrasonic pressure waves.[1,2] As an important detection technique for tracing gas, this technique is widely applied to atmospheric science.[1,3–13] When there is no problem of saturation, the response of photoacoustic spectroscopy is proportional to the excited laser power, and thus the photoacoustic performance can be improved by increasing the excited laser power. The commonly used methods mainly include two approaches: (i) a laser with higher power is used to increase the energy relaxation process. The high-power diode laser with 3.5 W is modulated to the mean output power of 1.5 W in the front of the photoacoustic cell by a square signal with a duty cycle of 50%, and is used to detect $NO_2$ with a detection limit of 54 ppt (1 s).[3,4] However, due to the large beam diameter and divergence, the high-power diode laser without any specific optic treatment is unsuitable for the photoacoustic system with conventional cavity structures and is not compatible with existing cavity technology.[14–17] However, the low power blue diode laser with output power in a range of mW is widely used and is compatible with different detection technologies for the cavity structure with a small internal diameter.[18–23] (ii) The photoacoustic cell can be optimized to improve the power by increasing the number of reflections. When the photoacoustic spectroscopy is combined with the cavity-enhanced absorption spectroscopy, the power in the cavity will be improved.[24–29] However, related research has mainly focused on the infrared band, while research on the ultraviolet band has been quite limited.

In this manuscript, we describe a new $NO_2$ photoacoustic sensor system with a high reflective mirror based on a low power blue diode laser at 403.56 nm, which can be used to optimize the photoacoustic cell. The power to excite the trace gas is enhanced through using the high reflective mirror to add a light path reflection. We design a photoacoustic cavity with a

*Project supported by the National Natural Science Foundation of China (Grant Nos. 91644107, 61575206, 51904009, and 41905130), the National Key Research and Development Program of China (Grant Nos. 2017YFC0209401, 2017YFC0209403, and 2017YFC0209902), and the Outstanding Young Talents Program of Anhui University, China (Grant No. gxyq2019022).

†Corresponding author. E-mail: phxie@aiofm.ac.cn

‡Corresponding author. E-mail: rzhu@aiofm.ac.cn

© 2020 Chinese Physical Society and IOP Publishing Ltd 

pool constant of 1450.64 (Pa·cm)/W and the signal sensitivity of 0.2562 μV/ppb. Comparing with a traditional photoacoustic system, the gain factor of the pool constant is 4.8, and the gain factor of signal sensitivity is 16. The temperature and humidity property of the new $NO_2$ photoacoustic sensor are analyzed, and the photoacoustic response and the drift of resonance frequency are also obtained.

## 2. Sensor design

### 2.1. Blue diode laser

Since the absorption coefficient is equal to the product of the absorption cross section and the concentration, the effective influence of the absorption cross section and interfering gas should be taken into consideration when selecting the laser. The absorption cross section of $NO_2$ for 390 nm–420 nm is shown in Fig. 1.[30] For comparison, the absorption cross section of $H_2O$ for 390 nm–420 nm is also shown in Fig. 1.[31] It can be seen that $NO_2$ has a strong absorption peak near 405 nm and the absorption of $H_2O$ is relatively small there. In addition, the absorption of other gases near 405 nm is not clear. For example, the absorption cross section of ozone is on the order of $10^{-23}$ cm.[32–34] By considering the influence of the absorption cross section and concentration, the blue diode laser (DL-405, Xilong, China) at 405 nm can be used to detect the concentration of $NO_2$ which thus avoids the absorption influence of $H_2O$ and other gases. The spectra obtained by a grating spectrometer (ULS2048, Avantes, China) show that the central wavelength of the blue diode laser is 403.56 nm and the half-peak full width is 0.84 nm. At this point, the effective absorption cross section of $NO_2$ at the central wavelength is $5.9485 \times 10^{-19}$ $cm^2$/mole. Since the output power of the blue diode laser at 120 mW is relatively low, the power after 50% square wave modulation is approximately 65.3 mW.

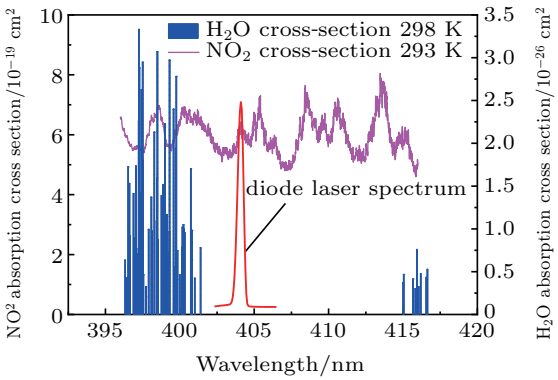



**Fig. 1.** Curves of the cross section *versus* wavelength of $NO_2$, $H_2O$, and diode laser spectrum.

### 2.2. $NO_2$ photoacoustic sensor with high reflective mirror

The $NO_2$ photoacoustic sensor with a high reflective mirror consists of a traditional photoacoustic cell, two buffer cavities with a gas inlet, and a gas outlet, a quartz glass plate, and a high reflective mirror. The schematic diagram of the sensor is shown in Fig. 2. The photoacoustic cell belongs to the class of the well-known Helmholtz resonator,[35,36] and is sealed by a quartz piece and a high-reflectivity mirror. The internal polished aluminum cylindrical channel of the photoacoustic cell has an inner diameter of 8 mm and the length of 120 mm. The cavity structure follows a horizontal assembly. Two buffer cavities, each with a length of 60 mm and a diameter of 25 mm, are both sealed by a quartz glass plate and a high-reflectivity mirror. The beam from the low power blue diode laser can easily pass through the photoacoustic cell by adjusting the flat reflector mirror and the high reflective mirror. The laser power is nearly doubled because of the high reflective mirror. When the laser is modulated at the resonance frequency of the photoacoustic cell, a standing sound wave is generated to be the maximum in the middle of the photoacoustic cell by absorbing a specific concentration of $NO_2$ gas. Hence, the condenser cylindrical microphone (MP201, Prestige, China) is installed in the middle of the photoacoustic cell to detect the acoustic pressure. At this time, the acoustic pressure can be changed by adjusting the high reflective mirror. Therefore, the performance of the photoacoustic sensor can be improved to detect the ambient atmospheric $NO_2$.

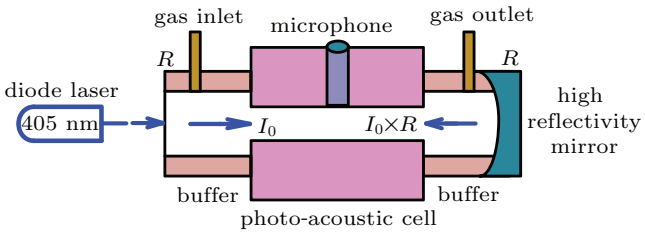



**Fig. 2.** The schematic diagram of the $NO_2$ photoacoustic sensor with high reflective mirror.

In order to obtain the reflectivity of the high-reflectivity mirror and ensure laser alignment and experimental consistency, a pair of high reflective mirrors are selected for calibrating and testing the cavity ring-down system (CRDS) that is designed and developed by our research group as shown in Fig. 3. The cavity length of the CRDS is 780 mm, and the sample length is 695 mm. By using the $NO_2$ gas with known concentration (0.204 ppm) as the standard gas, the corresponding coefficient is calculated to be $2.982 \times 10^{-6}$ $cm^{-1}$, and tests give the ring-down time as 4.2 μs. So according to Lambert's law with linear absorption, the reflectivity of the high reflective mirror is 99.959%. At this point, one of the high-reflectivity mirrors is selected for the system as described abover.

The system mainly depends on adjusting the ring down time of the cavity ring down system and observing the laser spots on the mirror to ensure the consistency of the light path of the series mode. In the series of optical paths, the photoacoustic cavity is outside of the ring down cavity and arranged independently, the photoacoustic cavity will be at the position to be passed through. It is actually sealed by the quartz

window, the verticality of the quartz window needs adjusting during the system adjustment, and the ring down cavity needs adjusting to determine whether the series of optical paths is collimated by determining the maximum ring down time. The optical path collimation is also applicable to the adjustment method.

The resonance frequency of the photoacoustic cell with a high-reflectivity mirror in the atmospheric environment is experimentally determined to be $f_0 \approx 1319.7$ Hz and the full width at half maximum (FWHM) of the frequency response curve (Fig. 4(a)) is $\Delta f \approx 145.4$ Hz, corresponding to a quality factor $Q = f_0/\Delta f \cong 9.1$. We compares this with the resonance frequency of the traditional photoacoustic cell with two quartz glass plates, which is experimentally determined to be $f_0 \approx 1346.8$ Hz and the FWHM of the frequency response curve (Fig. 4(b)) is $\Delta f = 84.9$ Hz, corresponding to a quality factor $Q = f_0/\Delta f \cong 15.9$. The difference in $Q$ between the new photoacoustic system and traditional photoacoustic system comes from the sealing mode and microphone sensitivity. The two ends of the traditional photoacoustic cavity are sealed by quartz window plates, while one end of the high-reflective photoacoustic cavity is replaced by a high-reflectivity mirror. It can be seen that the new photoacoustic system has advantages in both response amplitude and frequency shift resistance.

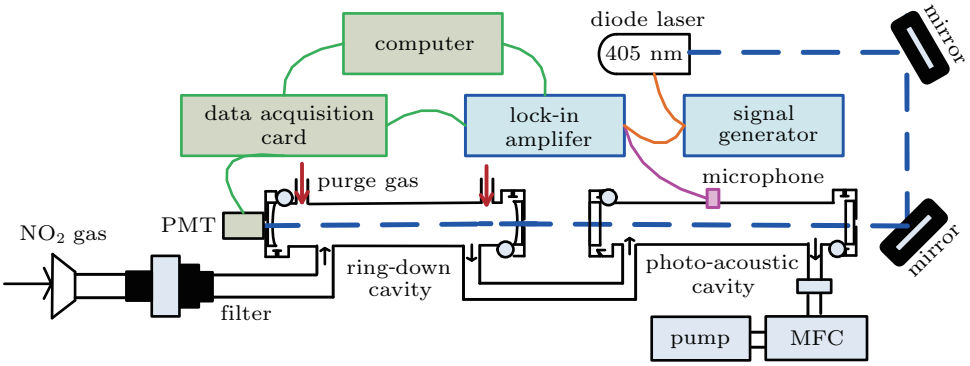



**Fig. 3.** Experimental diagram of $NO_2$ photoacoustic sensor with high reflective mirror.

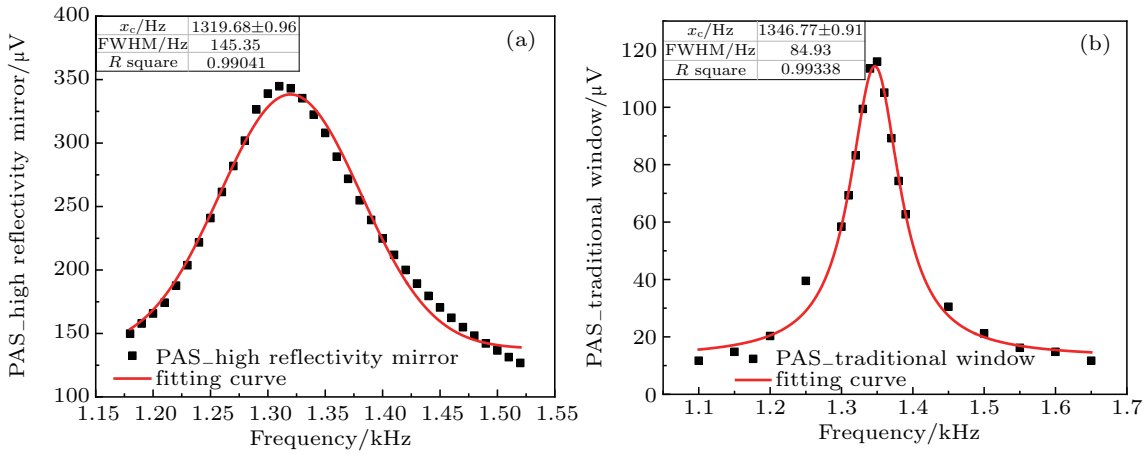



**Fig. 4.** Response frequency curve for (a) photoacoustic cell with a high reflective mirror and (b) traditional photoacoustic cell.

## 3. Experimental setup of sensor system

The experimental setup of the $NO_2$ photoacoustic sensor with a high-reflectivity mirror is depicted in Fig. 5. It mainly includes the photoacoustic sensor, temperature control system, and humidity control system. The photoacoustic sensor consists of a blue diode laser, a photoacoustic cell, an air intake unit, a sound acquisition system, and a data processing system. The self-developed function generator unit generates two channels of 0 V–1 V square waves with 50% duty cycle. The frequency is set at the resonance frequency of the photoacoustic cell. One channel is used to modulate the blue diode laser, and the other channel is used as the phase-locked frequency of the amplifier (OE1022D, Saien, China). The sound signal is collected by the microphone. A tetrafluoroethylene tube is used to form the intake unit in order to reduce the adsorption effect of the inner wall on $NO_2$.

The pure $N_2$ and $NO_2$ sample gases with 0.204 ppm are used as a mixed source gas. The mixed gases with different concentrations, water vapor, and temperatures are configured by controlling the flow rate and thermometer. The total flow should be controlled at 1 L/min by controlling the flow rate of

the pure nitrogen, water vapor, and $NO_2$. The heating device consists of a copper spiral tube, flexible silicone rubber heating tablets, high temperature insulation materials, a temperature probe, and temperature controllers. The length and diameter of the copper spiral tube are 30 cm and 6.5 cm respectively. The resistance and the power of the flexible silicone rubber heating tablets are 396 Ω and 120 W respectively. High temperature insulation materials consist of quartz fiber and cotton insulation. The experimental system test site is shown in Fig. 6.

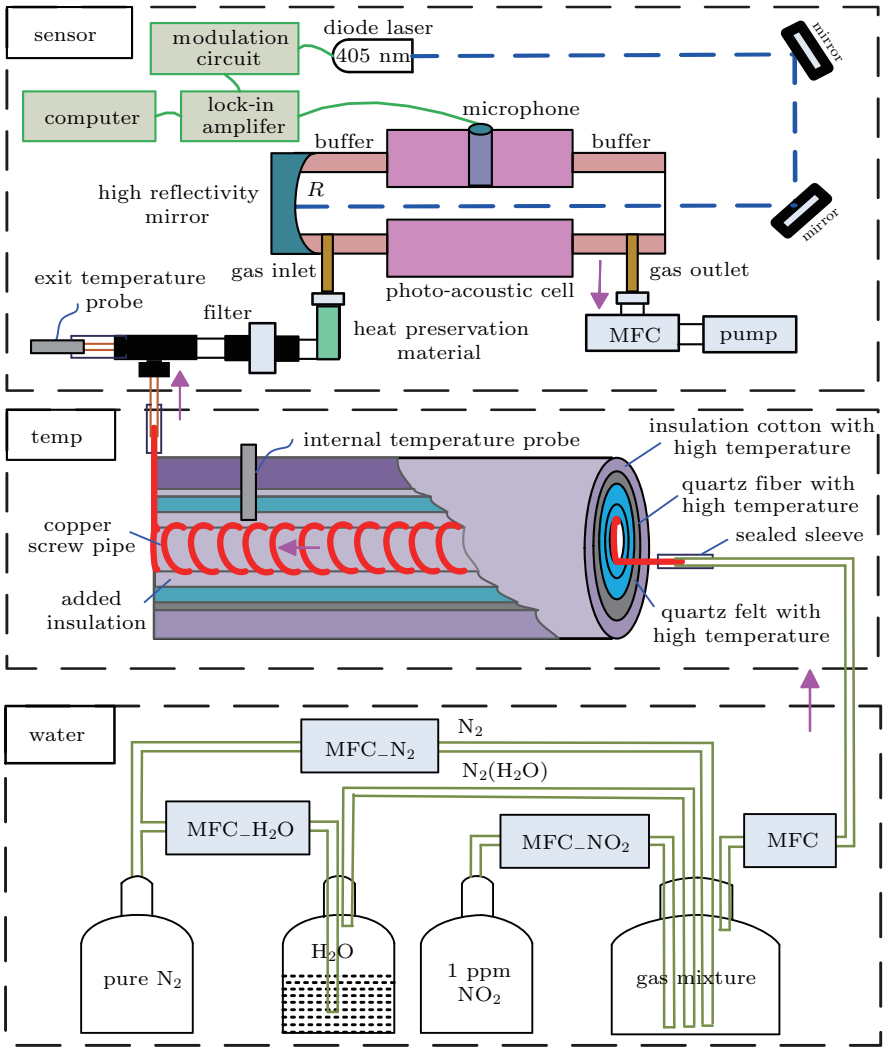



**Fig. 5.** Experimental system of new $NO_2$ photoacoustic sensor with high reflective mirror based on low power blue diode laser.

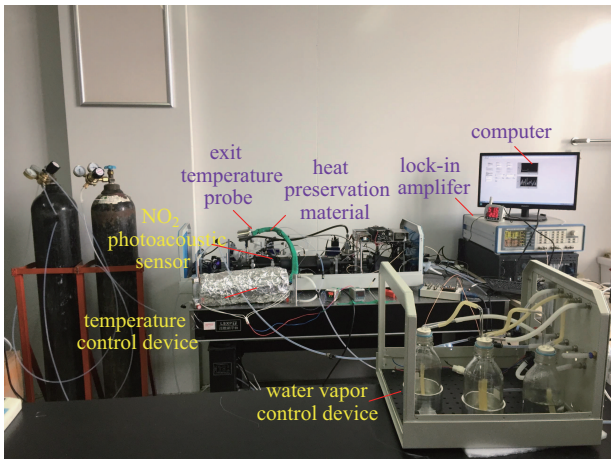



**Fig. 6.** Experimental system test site.

## 4. Results and discussion

### 4.1. Photoacoustic cell

The background noise and excitation signal are tested with 3.4-ppm $NO_2$. The background noise of the system is $3.212 \pm 0.188$ μV, compared with the excitation signal of $109.217 \pm 1.043$ μV. The data in this paper are all computed by subtracting the local noise. The specific background noise information is shown in Fig. 7.

When the sensor is first filled with 0.204-ppm $NO_2$, the signal value from the photoacoustic sensor is 26.11 μV. The measurements are carried out at atmospheric pressure and room temperature. The absorption cross section of $NO_2$ is $5.9485 \times 10^{-19}$ $cm^2$/mole, the sensitivity of the microphone is 53.7 mV/Pa, and the laser power is doubled to 112.4 mW

by the high-relectivitiy mirror, so the pool constant of the photoacoustic cell can be calculated from the following equation:

$$C_{\text{cell}} = \frac{S_{\text{PA}}}{S_{\text{m}} \alpha P} = 1450.64 \text{ Pa} \cdot \text{cm/W}, \quad (1)$$

where $C_{\text{cell}}$ (in units Pa·cm/W) is the pool constant of the photoacoustic cell, $S_{\text{PA}}$ (in unit μV) the photo-acoustic response, $S_{\text{m}}$ (mV/Pa) the sensitivity of the microphone, $\alpha$ ($\text{cm}^{-1}$) the absorption coefficient of $NO_2$, and $P$ (W) the power of the laser in the cavity.

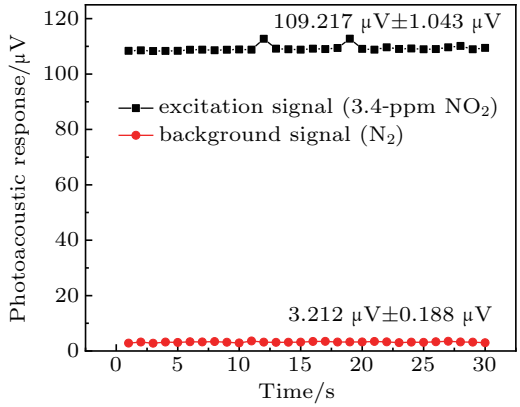



**Fig. 7.** Background noise and excitation signal varying with time.

### 4.2. Photoacoustic response

In order to evaluate the performance of the sensor in terms of accuracy and linearity, seven different concentration levels of the $NO_2$ sample gas ranging from 17 ppb to 340 ppb are fed into the sensor. The signal amplitudes from the sensor are shown in Fig. 8(a). The sensor is operated at atmospheric pressure and room temperature. The average data points of the signal are recorded continuously for 10 min at each concentration level. By fitting the experimental data, the system shows a good linearity, and the slope is 0.2562 μV/ppb. The experimental slope is consistent with the theoretical slope. The detection linearity is in excellent agreement with the signal sensitivity factor of 0.2560 μV/ppb after considering the interference. Comparing with the ideal curve, $R^2$ reaches to 0.99859, and the data error is less than 5%.

The performance test of a traditional photoacoustic cell sealed by two quartz glass plates is conducted and the result is shown in Fig. 8(b). In the traditional photoacoustic system the blue light diode laser is also used. The main structure is completely consistent with the highly reflective photoacoustic cavity, and their differences lie in the sealing mode and microphone sensitivity. The two ends of the traditional optical-acoustic cavity are sealed by quartz window plates, while one end of the highly reflective photoacoustic cavity is replaced by a high-reflectivity mirror. The sensitivity of the traditional photoacoustic system is 40.2 V/Pa, while that of the high reflective photoacoustic cavity is 53.7 V/Pa. The pool constant of the photoacoustic cell calculated from Eq. (1) is 300.24 (Pa·cm)/W.[5,6] By comparison, the photoacoustic sensor effectively enhances the value of the pool constant from 300.24 (Pa·cm)/W to 1450.64 (Pa·cm)/W, corresponding to a gain factor of 4.8. The signal sensitivity of the traditional photoacoustic sensor is 0.016 μV/ppb. The photoacoustic sensor with high reflective can effectively enhance the value of the signal sensitivity from 0.016 μV/ppb to 0.2562 μV/ppb, corresponding to a gain factor of 16. By taking into account the doubling of optics power, we find that the responsivity of the highly reflective photoacoustic cavity is theoretically 12.90 times higher than that of the traditional photoacoustic cavity. There is a certain difference between the two, which may be caused by cavity processing, laser collimation, and other factors. It may also be caused by the difference in $NO_2$ standard gas when the two systems are not synchronized, because $NO_2$ standard gas has certain adsorption characteristics. In summary, the photoacoustic performance is greatly improved.

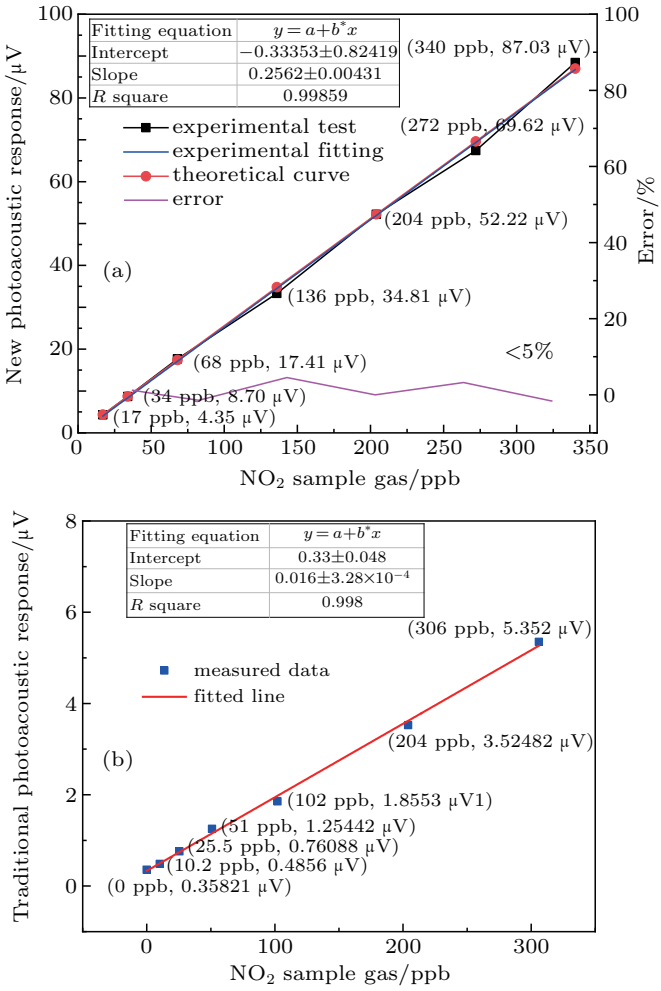



**Fig. 8.** Photoacoustic response for (a) new sensor and (b) traditional sensor.

### 4.3. Discussion of influence factor

Standard $NO_2$ gas is selected as the standard gas to be used in the experiment; its concentration is 0.34 ppm, and the humidity of the gas remains at 0%. The experiments are car-

ried out at atmospheric pressure and room temperature. By comparison, the responsivity values of the photoacoustic sensor under temperatures ranging from 20.9 °C to 31.4 °C are shown in Fig. 9(a). Photoacoustic response should increase with temperature rising. Compared with the resonance frequency of 1.30 kHz at 20.9 °C and 23.6 °C, the resonance frequency is 1.31 kHz at 24.8 °C, and 1.32 kHz at 26.5 °C, 28.4 °C, and 31.4 °C. The resonance frequency tends to shift with temperature rising.

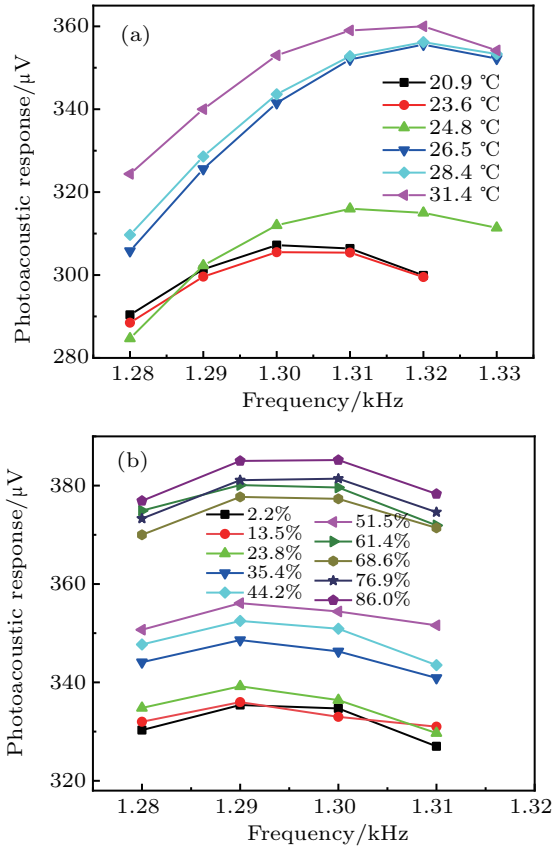



**Fig. 9.** (a) Relationship between photoacoustic response, resonance frequency, and temperature. Photoacoustic response should increase with temperature rising, and the resonance frequency tends to drift with temperature rising. (b) Relationship between photoacoustic response, resonance frequency, and humidity. Photoacoustic response increases with humidity increasing, and humidity has no effect on resonant frequency.

In the same way the photoacoustic sensor is filled with the $NO_2$ sample gas at a specific temperature and concentration. Similarly, the $NO_2$ sample gases with various values of the humidity at a specific temperature fill the photoacoustic sensor, respectively, in experiments. By comparison the signals of the photoacoustic sensor under various values of the humidity ranging from 0% to 90% are shown in Fig. 9(b). The photoacoustic response should increase with humidity increasing. However, the resonance frequency does not vary with humidity. That is, humidity has no effect on the resonant frequency of the photoacoustic cell. In addition the characteristics of temperature and humidity are obtained at atmospheric pressure to quantify the photoacoustic response and the drift of resonance frequency.

## 5. Calibration study on influence of temperature and humidity

In this paper, the neural network algorithm is introduced into the later data processing of the photoacoustic system, and the self-designed cavity ring down system is selected as the reference measurement system to carry out the research on the correction method of the influence of temperature and humidity on the photoacoustic system. The designed parameter data have three inputs and one output. The three inputs are light acoustic response, temperature, and humidity inputs. The one output is the true value output of the cavity attenuation system. A three-layered BP neural network is used to carry out the correction study, and the hidden layer node is set at 15.

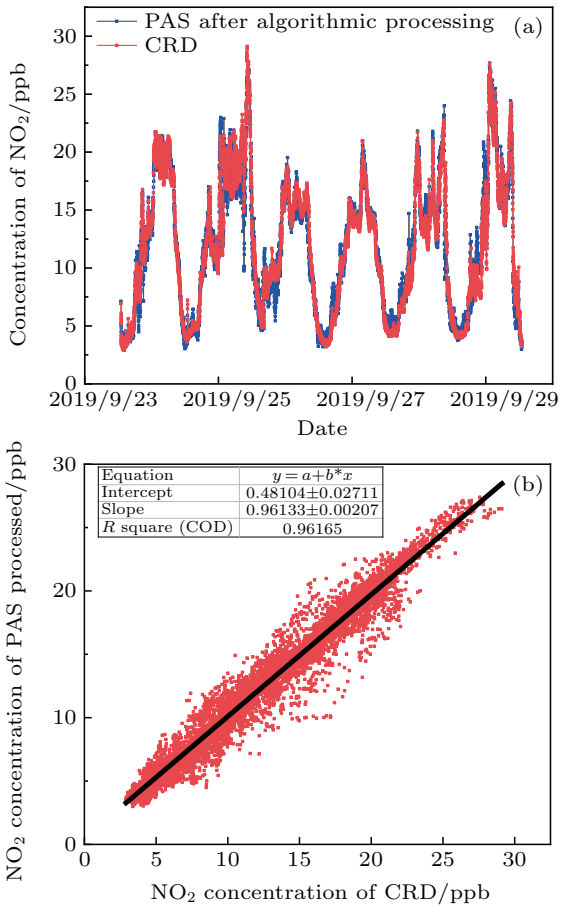



**Fig. 10.** Comparison and correlation between photoacoustic samples and reference ture values after correction.

The photoacoustic system and cavity ring down system are used to measure the concentration of $NO_2$ in the ambient atmosphere in Dongpu reservoir (latitude 31.89, longitude 117.20) in Hefei, Anhui Province, China from September 23rd to 30th, 2019. The comparison and correlation results of the simulation model of the neural network are shown in Fig. 10. The corresponding correlation $R^2$ is 0.96165, the slope is $0.96133 \pm 0.00207$, and the intercept is $0.48104 \pm 0.02711$. It can be seen that after the neural network correction, the sample is highly correlated with the reference quantity and the cor-

rection result is good. Thus, the neural network correcetion can be used as the correction algorithm of the photoacoustic system to adapt the influence of temperature and humidity on resonance frequency drift.

## 6. Conclusions

We demonstrate a $NO_2$ photoacoustic sensor system with a high-reflectivity mirror based on the low power blue diode laser at 403.56 nm. The high-reflectivity mirror enhances the power of the diode laser by increasing the number of reflections, resulting in the pool constant gain factor of 4.8 and a signal sensitivity gain factor of 6.4. Compared with that of a traditional photoacoustic sensor, the pool constant of the photoacoustic cell is improved from 300.24 (Pa·cm)/W to 1450.64 (Pa·cm)/W, and the signal sensitivity of the photoacoustic sensor is improved from 0.016 μV/ppb to 0.2562 μV/ppb. The properties of temperature and humidity of the new $NO_2$ photoacoustic sensor are analyzed. The features of photoacoustic response and the drift of resonance frequency are also obtained and algorithm is corrected. The above research provides a new method and concept for further developing the $NO_2$ photoacoustic sensors.

## Acknowledgment

The authors thank the Key Laboratory of Environmental Optics & Technology, Anhui Institute of Optics and Fine Mechanics, Chinese Academy of Sciences for their contribution to this work.

## References

[1] Miklos A, Hess P and Bozoki Z 2001 *Rev. Sci. Instrum.* **72** 1937
[2] Sim J Y, Ahn C G, Huh C, *et al.* 2017 *Sensors* **17** 80
[3] Yin X K, Dong L, Wu H P, *et al.* 2017 *Opt. Express* **25** 32581
[4] Yin X K, Dong L, Wu H P, *et al.* 2017 *Sens. Actuators B-Chem.* **247** 329
[5] Jin H W, Hu R Z, Xie P H, *et al.* 2019 *Acta Phys. Sin.* **68** 070703 (in Chinese)
[6] Jin H W, Hu R Z, Xie P H, *et al.* 2019 *Spectrosc. Spect. Anal.* **39** 1993 (in Chinese)
[7] Wang L, Wang W G and Ge M F 2012 *J. Environ. Sci.* **24** 1759
[8] Ma Y F, He Y, Yu X, *et al.* 2016 *Sens. Actuators B-Chem.* **233** 388
[9] Elefante A, Giglio M, Sampaolo A, *et al.* 2019 *Anal. Chem.* **91** 12866
[10] Li S Z, Dong L, Wu H P, *et al.* 2019 *Anal. Chem.* **91** 5834
[11] Zhang C X, Liu C, Hu Q H, *et al.* 2019 *Light: Sci. & Appl.* **8** 100
[12] Yin X K, Wu H P, Dong L, *et al.* 2020 *ACS Sens.* **5** 549
[13] Song W, Guo G D, Wang J, *et al.* 2019 *ACS Sens.* **4** 2697
[14] Ajtai T, Kiss-Albert G, Utry N, *et al.* 2019 *J. Environ. Sci.* **83** 96
[15] De Cumis M S, Viciani S, Borri S, *et al.* 2014 *Opt. Express* **22** 28222
[16] Pourhashemi A, Farrell R M, Cohen D A, *et al.* 2015 *Appl. Phys. Lett.* **106** 111105
[17] Pourhashemi A, Farrell R M, Cohen D A, *et al.* 2016 *Electron. Lett.* **52** 2003
[18] Fuchs H, Dube W P, Lerner B M, *et al.* 2009 *Environ. Sci. & Technol.* **43** 7831
[19] Li J L, Wang W G, Li K, *et al.* 2019 *J. Environ. Sci.* **76** 227
[20] Li Z Y, Hu R Z, Xie P H, *et al.* 2019 *Atmos. Meas. Tech.* **12** 3223
[21] Singh S, Fiddler M N, Smith D, *et al.* 2014 *Aerosol Sci. Technol.* **48** 1345
[22] Taha Y M, Odame-Ankrah C A and Osthoff H D 2013 *Chem. Phys. Lett.* **582** 15
[23] Washenfelder R A, Wagner N L, Dube W P, *et al.* 2011 *Environ. Sci. & Technol.* **45** 2938
[24] Chen K, Gong Z F and Yu Q X 2018 *Sens. Actuators A-Physical* **274** 184
[25] He Q, Zheng C T, Lou M H, *et al.* 2018 *Opt. Express* **26** 15436
[26] He Y, Ma Y F, Tong Y, *et al.* 2018 *Opt. Express* **26** 9666
[27] Pan Y F, Dong L, Wu H P, *et al.* 2019 *Atmos. Meas. Tech.* **12** 1905
[28] Patimisco P, Borri S, Galli I, *et al.* 2015 *Analyst* **140** 736
[29] Wojtas J, Gluszek A, Hudzikowski A, *et al.* 2017 *Sensors* **17** 513
[30] Voigt S, Orphal J and Burrows J P 2002 *J. Photochem. Photobiol. A-Chem.* **149** 1
[31] Rothman L S, Gordon I E, Barber R J, *et al.* 2010 *J. Quant. Spectrosc. & Radiat. Transfer* **111** 2139
[32] Chen L W, Ondarts M, Outin J, *et al.* 2018 *J. Environ. Sci.* **74** 58
[33] Deng Y Y, Li J, Li Y Q, *et al.* 2019 *J. Environ. Sci.* **75** 334
[34] Dong L, Tittel F K, Li C G, *et al.* 2016 *Opt. Express* **24** A528
[35] Zeninari V, Kapitanov V A, Courtois D, *et al.* 1999 *Infrared Phys. Technol.* **40** 1
[36] Zheng H D, Lou M, Dong L, *et al.* 2017 *Opt. Express* **25** 16761